Medicinal Chemistry Research (2025) 34:895–909
https://doi.org/10.1007/s00044-025-03386-5

MEDICINAL CHEMISTRY RESEARCH

ORIGINAL RESEARCH ARTICLE

An evaluation of spirooxindoles as blocking agents of SARS-CoV-2 spike/ACE2 interaction: synthesis, biological evaluation and computational analysis

Albert Enama Ehinak[1,2] · Maloba M. M. Lobe[1,2] · Donatus B. Eni[1,2] · Conrad V. Simoben[1,3] · Ian Tietjen[4] · Mathieu J. Mbenga Tjegbe[1] · Joel Cassel[4] · Joseph M. Salvino[4] · Luis J. Montaner[4] · Wolfgang Sippl[5] · Simon M. N. Efange[1,6] · Fidele Ntie-Kang[1,2,5]

Received: 28 January 2025 / Accepted: 10 February 2025 / Published online: 23 February 2025

Abstract

Severe acute respiratory syndrome coronavirus 2 (SARS-CoV-2) has gained significant public health attention owing to its devastating effects on lives and livelihoods worldwide. Due to difficult access to vaccines in many developing countries and the inefficiency of vaccines in providing complete protection even with fully vaccinated persons, there remains the need for the development of novel drugs to combat the disease. This study describes the in vitro activity of a library of fifty-five spiro-fused tetrahydroisoquinoline–oxindole hybrids (spirooxindoles) as potential blocking agents of the interaction between the SARS-CoV-2 viral spike and the human angiotensin-converting enzyme 2 (ACE2) receptor, essential for viral transmission. The synthesis was conducted by the Pictet-Spengler condensation of phenethylamine and isatin derivatives, while the screening against spike-ACE2 interaction was done using our previously described AlphaScreen fluorescent assay. The in vitro screening identified compound (**11j**) as the most active, showing a 50% inhibitory concentration (IC_{50}) of 3.6 µM against SARS-CoV-2 spike/ACE2 interaction. Structure-activity relationships explained via molecular docking studies and the computation of binding free energy of each compound with respect to the spike/ACE2 protein-protein interaction showed that the most active compound possesses a bulky naphthyl group, which addresses voluminous hydrophobic regions of the ACE2 binding site and interacts with the hydrophobic residues of the target. Therefore, these compounds could be potentially useful in searching for SARS-CoV-2 spike/ACE2 interaction blocking agents.

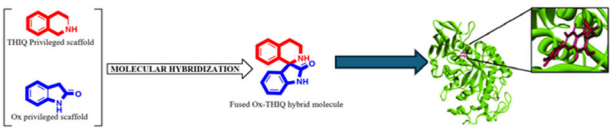

Keywords Antivirals · Hybrids · SARS-CoV-2 · Spike/ACE2 · Spirooxindoles

These authors contributed equally: Albert Enama Ehinak, Maloba M. M. Lobe

✉ Simon M. N. Efange
smbuangalefange@gmail.com

✉ Fidele Ntie-Kang
fidele.ntie-kang@ubuea.cm

[1] Center for Drug Discovery, Faculty of Science, University of Buea, P. O. Box 63, Buea, Cameroon

[2] Department of Chemistry, Faculty of Science, University of Buea, P. O. Box 63, Buea, Cameroon

[3] Structural Genomics Consortium, University of Toronto, Toronto, ON M5G 1L7, Canada

[4] The Wistar Institute, Philadelphia, PA, USA

[5] Institute of Pharmacy, Martin-Luther University Halle-Wittenberg, Kurt-Mothes-Str. 3, 06120 Halle (Saale), Germany

[6] Chemical Bioactivity Information Center, University of Buea, Buea, Cameroon

Introduction

Severe acute respiratory syndrome coronavirus 2 (SARS-CoV-2), the agent of coronavirus disease 19 (COVID-19), has emerged as a very important public health concern, requiring the need to develop new antiviral drugs because approved vaccines are less efficacious in preventing transmission [1]. Since its outbreak, there have been over 770 million confirmed cases of SARS-CoV-2 globally, resulting in about 7 million deaths [2]. One drug discovery approach against this viral transmission is to disrupt its recognition of the membrane-bound angiotensin-converting enzyme 2 (ACE2) by the viral spike protein, thereby hindering the interaction of the receptor binding domain (RBD) located at its S1 subunit, which is responsible for cellular entry [3–6].

Privileged scaffolds for small molecule discovery of SARS-CoV-2 spike/ACE2 protein-protein interaction include isatin derivatives [7–10], peptides [11, 12], mono- and di-thiols [13], the PARP inhibitor rucaparib [14], as well naturally occurring compounds [15–21]. Spirocyclic compounds, especially spirooxindoles, have gained significant interest in medicinal chemistry as privileged scaffolds owing to their unique three-dimensional structures and the broad spectrum of biological activities, including antiviral properties [22–31].

Interest in spiro compounds and indoles and oxindoles as potential SARS-CoV-2 inhibitors has been spurred by recent literature evidence [22–31]. It was reported that spirooxindoles based on uracil derivatives could inhibit the growth of the SARS-CoV-2 virus by targeting RNA polymerase and spike glycoprotein [22]. Besides, 3-alkenyl-2-oxindoles, isatins, spiro-3-indolin-2-ones, indoles and oxindole derivatives (see Fig. S1, Supplementary Data) have exhibited antiviral properties against SARS-CoV-2, the most promising spiro-3-indolin-2-one compound being 3.3 and 4.8 times the potency of the standard references, chloroquine and hydroxychloroquine, in their growth inhibition potency against SARS-CoV-2 [23, 24, 28, 29]. An examination of the recent literature seems to point to the fact that both chloroquine and hydroxychloroquine inhibit the growth of SARS-CoV-2 in vitro by blocking the interaction between the viral spike protein and the human ACE2 receptor, although both drugs have not yet demonstrated in vivo efficacy in clinical trials [32–38]. Oxindole-based compounds have been shown to inhibit the SARS-CoV-2 main protease (M^{pro}) [25, 26]. It was demonstrated that spirooxindoles based on phenylsulfonyl moiety could inhibit the growth of both SARS-CoV-2 and MERS-CoV-2 [27]. The natural products (oxindole alkaloids) [30, 39] from *Uncaria* species have been investigated as potential lead compounds for the discovery of anti-SARS-CoV-2 agents, while labdane-oxindole hybrid compounds were effective in inhibiting the growth of the Chikungunya virus [31]. In particular, a 7-chloro-oxindole (*E*)-42 was shown to be a potent inhibitor against two low-passage CHIKV isolates from human patients, with EC_{50} values of 1.55 µM and 0.14 µM against the variants CHIKV-122508 and CHIKV-6708, respectively. This justifies our interest in investigating spirooxindole hybrids that could inhibit viral growth, targeting SARS-CoV-2 enzymes.

Owing to the demonstrated activities of spirooxindoles based on the phenylsulfonyl moiety to inhibit the growth of SARS-CoV-2 and MERS-CoV-2 [27], as well as the activities of oxindole alkaloids against SARS-CoV-2 [30, 39] we have engaged in the investigation of their hybrids (spiro-oxindoles) against the viral protein targets. Since the binding of the viral spike protein with the human ACE2 receptor is vital for viral transmission, we carried out this investigation to identify potential entry inhibitors that would potentially prevent viral transmission. The present study focuses on the molecular hybridization approach for the design and synthesis of a series of spirooxindoles based on the recently described 3′,4′-dihydro-2′*H*-spiro[indoline-3,1′-isoquinolin]-2-ones (DSIIQs), by coupling two scaffolds, i.e. tetrahydroisoquinoline (THIQ) and oxindole (OX), as spike/ACE2 interaction inhibitors, which could potentially prevent transmission. This could be by binding to the angiotensin II site (substrate binding site) to modulate the human receptor and potentially prevent it from recognizing the receptor-binding domain of the viral spike.

Results and discussion

Chemistry

The synthesis of fifty of the test compounds (Fig. 1) has been previously described [40–42], while an additional 5 compounds were newly synthesized and tested. The general synthetic schemes for both the major fragments (see Scheme S1, Supplementary Data) and the 5 target compounds (**12a, 13l, 14h, 17c**, and **17d**) are shown in Scheme 1 in the Experimental section. The syntheses of both the target compounds (spirooxindoles) and the major intermediates are represented in Scheme 1 and S1 (Supplementary Data), respectively. The intermediate methoxy phenethylamines (**5a, b**) were prepared from commercially available benzaldehydes. The appropriate substituted benzaldehydes were transformed into beta-nitro styrenes (**4a, b**) in an adol-type condensation reaction of benzaldehyde and nitromethane. Subsequent Clemmensen reduction (using zinc dust in concentrated hydrochloric acid) of the beta-nitro styrenes afforded the substituted phenethylamines (**5a, b**) illustrated in the method a) of Scheme S1 (Supplementary Data). The isatin derivatives (**7**) were prepared by treating commercially available isatins with substituted

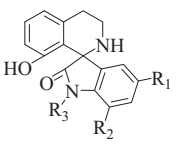

10d, f - h, j - l

a: $R_1 = R_2 = R_3 = H$
b: $R_1 = Cl$; $R_2 = R_3 = H$
c: $R_1 = R_2 =$Br; $R_3 = H$
d: $R_1 = R_2 = H$; R_3 = 4-fluorobenzyl
e: $R_1 = R_2 = H$; R_3 = 4-chlorobenzyl
f: $R_1 = R_2 = H$; R_3 = 4-bromobenzyl
g: $R_1 = R_2 = R_3$ = 3,4-dichlorobenzyl

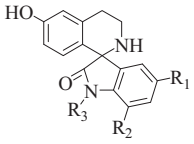

11a - m

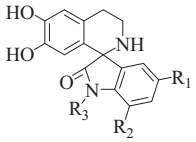

12a - c

h: $R_1 = R_2 = H$; R_3 = 4-methylbenzyl
i: $R_1 = R_2 = H$; R_3 = 4-nitrobenzyl
j: $R_1 = R_2 = H$; R_3 = (2-naphthyl)methyl
k: $R_1 = Cl$; $R_2 = H$; R_3 = 4-fluorobenzyl
l: $R_1 = Cl$; $R_2 = H$; R_3 = 4-chlorobenzyl
m: $R_1 = Cl$; $R_2 = H$; R_3 = 4-methylbenzyl

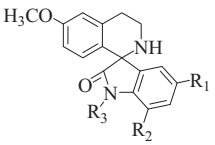

13a - e, k, l

a : $R_1 = R_2 = R_3 = H$
b : $R_1 = Cl$; $= R_2 = R_3 = H$
c : $R_1 = R_2 = Br$; $R_3 = H$
d : $R_1 = R_2 = H$; R_3 = 4-fluorobenzyl
e : $R_1 = R_2 = H$; R_3 = 4-methylbenzyl
f : $R_1 = Cl$; $R_2 = H$; R_3 = 4-brombenzyl

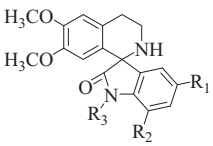

14a - k, m - n

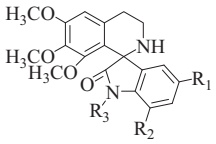

15a - e

h : $R_1 = CH_3$; $R_2 = H$; R_3 = 4-fluorobenzyl
j : $R_1 = R_2 = Br$; R_3 = phenylacetamido
k :$R_1 = R_2 = H$; R_3 = Phenyl
l : $R_1 = CH_3$; $R_2 = R_3 = H$
m : $R_1 = NO_2$; $R_2 = R_3 = H$
n : $R_1 = F$; $R^2 = R_3 = H$

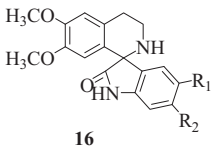

16

a : $R_1 = R_2 = F$
b : $R_1 = F$; $= R_2$ = piperidin-1-yl

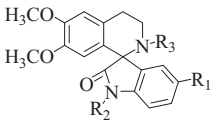

17c - e

c : $R_1 = H$; R_2 = 4-methylbenzyl; R_3 = ethylacetamido
d : $R_1 = H$; R_2 = 4-methylbenzyl; $R_3 = CH_3$
e : $R_1 = NO_2$; $R_2 = H$; $R_3 = CH_3$

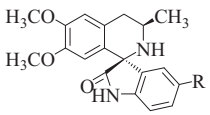

18

a: R = Cl
b: R = I

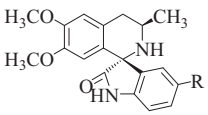

19

a: R = Cl
b: R = I

Fig. 1 Showing the fifty-five spirooxindoles that were tested against SARS-CoV-2 spike/ACE2 inhibitory activity. The synthesis of fifty compounds was previously described [40–42], while five additional compounds were newly synthesized as described in the Experimental Section

benzyl halides, in the presence of K_2CO_3, KI, and DMF as indicated in method b) of Scheme S1 (Supplementary Data). Phenolic Pictet–Spengler condensation reaction (using triethylamine in ethanol) of dopamine and substituted isatin afforded the target compound (**12**) as shown in method A of Scheme 1. Compounds (**13**) and (**14**) were prepared by the Pictet–Spengler condensation reaction (using polyphosphoric acid at 100 °C) of methoxyphenethylamine and the corresponding isatins, as shown method B Scheme 1. Compound (**17c**) was prepared by treating 6′,7′-dimethoxy-1-(4-methylbenzyl)-3′,4′-dihydro-2′H-spiro[indoline-3,1′-isoquinolin]-2-one with ethyl isocyanate in acetonitrile, while compound (**17d**) was synthesized by treating 6′,7′-dimethoxy-1-(4-methylbenzyl)-3′,4′-dihydro-2′H-spiro[indoline-3,1′-isoquinolin]-2-one with formaldehyde and formic acid as indicated in method C of Scheme 1.

Activities observed in the AlphaScreen assay

For the synthesized compounds, the 50% inhibitory concentrations (IC_{50} values) for spike/ACE2 binding (AlphaScreen) are shown in Table 1, alongside the best docking score for each ligand. The cut-off concentrations to distinguish between active, moderately active, and inactive ligands for SARS-CoV-2 fluorescent assay were adopted from recent literature [43] and are summarized in Table S2

Scheme 1 Synthesis of target compounds

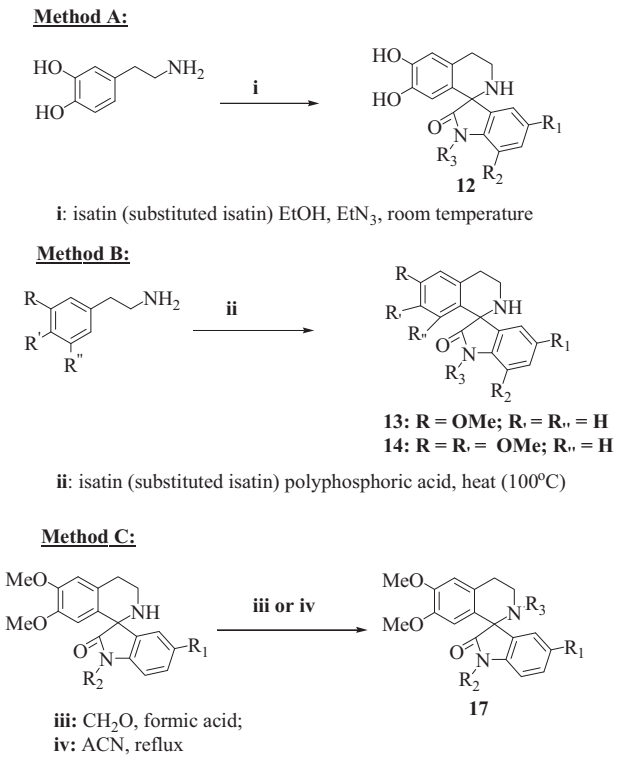

(Supplementary Data). Often, docking algorithms are good at predicting the binding mode of compounds towards a protein target (docking poses) but lack the ability to predict the affinity of the compounds to the protein. Docking scoring functions often perform well only when the compounds in the training sets are within the same domain of applicability as the compounds being investigated [44]. To overcome this problem, the docked poses are often "re-scored" by performing binding free-energy calculations and the use of solvation models that have been tested against a broad range of proteins and compound datasets [45].

On this basis, the ligands were classified into three categories: A (active, with $IC_{50} < 10\,\mu M$), B (moderately active, with $10\,\mu M < IC_{50} < 20\,\mu M$), and C (inactive, with $IC_{50} > 20\,\mu M$) for the spike/ACE2 assay. In parallel, the compounds were tested in the M^{pro} assay and all showed to be inactive (Table S1, See Supplementary Data). The classification of the ligands into categories A to C is shown in Table S1 (Supplementary Data). Of the fifty-five tested spirooxindoles, fifteen fell under category A, including **10f, 10h, 10j, 10l, 11j, 11l, 11m, 12b, 12c, 13l, 14f, 14h, 14j, 15c** and **16b** the most active compound being **11j** ($IC_{50} = 3.6\,\mu M$). There were nine compounds in category B, which include **10g, 11e, 11g, 12a, 14k, 14m, 15b, 18b**, and **19b**. The remaining compounds were inactive (category C). We could further identify a subset of non-selective compounds in categories A and B (referred to as A′ and B′, respectively), which we could define as active compounds and moderately active compounds against spike/ACE2, which could contain some pharmacophore features required for binding to M^{pro}. These are compounds that could be slightly modified to derive dual inhibitors of spike/ACE2 and M^{pro}. Category A′ includes compounds **10f, 12b, 12c**, and **14j**, while category B′ includes compounds **10g, 18b**, and **19b**. Our discussion of the structure-activity relationships will focus on the common features of compounds in categories A, A′, B, and B′ which are absent from category C and vice versa. Although there was no correlation between the activities of the compounds and their docking scores towards the spike/ACE2 site, the orientations of the top-scoring poses could carefully explain the structure-activity relations. Figure S2 (Supplementary Data) shows a superposition of all the active compounds, indicating that all compounds adopted the same binding mode within the angiotensin II site. A careful observation of the spike/ACE2 binding site reveals that most of the active compounds interact with the residues Asn376 by two H-bonds, Asp364 by one H-bond, as well as Ala330 with two H-bonds and Trp329 through π-π stacking.

It was observed that the most active compound (**11j**, $IC_{50} = 3.60\,\mu M$) interacted with Arg375 via the N-H of the isoquinoline moiety (Fig. 2), while the naphthyl group made several arene-H interactions with Asp332. Although these amino acids make similar interactions with almost all the actives, compound **11j** distinguishes itself by the strong hydrophobic interactions resulting from the interaction field produced by the naphthyl moiety. This matches with the strong hydrophobic patch created by the amino acids Phe22, Ser26, Leu333, and Ile361 (shown in Figs. 2B, C), which is an indication that the activity of this compound could be driven by the strong hydrophobic interactions between the naphthyl moiety and this patch. This suggests that more active compounds could be designed and synthesized by introducing other hydrophobic groups around the naphthyl (F, CH_3, Cl, CF_3, Br, etc.) moiety, a feature that is conspicuously absent from the moderately active and inactive compounds.

The 8-hydroxy isomer of the most active compound (**11j**), i.e. compound **10j** was shown to be about twofold less active ($IC_{50} = 7.4\,\mu M$). A superposition of the two isomers has been shown in the angiotensin II site in Fig. 2. While the 6-hydroxy group in compound **11j** is free to make H-bond interactions with the protein backbone, this possibility is hindered in compound **10j**, which rather forms intramolecular H-bonding with the carbonyl of the oxindole moiety. This could explain the observed activity of compound **11j** compared with compound **10j**. The top-scoring poses of the rest of the two molecules show almost perfect superposition (Fig. 3). The rescoring by MM-GBSA revealed that amongst the fifteen compounds of category

Table 1 Biological assay results, docking and MM-GBSA results for spike/ACE2

Compound ID	Screening and Docking		Rescoring with MM-GBSA	
	IC_{50} (μM)	Glide (SP) Score	ΔG_{bind} (kcal/mol)	ΔG_{solv} (kcal/mol)
10d	20.4	−6.75	−40.98	39.22
10f	9.7	−6.42	−26.69	48.10
10g	14.7	−6.52	−35.64	46.93
10h	9.8	−6.73	−41.89	33.29
10j	7.4	−7.12	−30.64	46.12
10k	35.2	−5.89	−40.644	40.64
10l	6.1	−6.15	−21.08	53.33
11a	71.3	−6.58	−20.04	50.04
11b	>100	−6.10	−33.34	38.62
11c	>100	−5.36	−22.04	37.64
11d	70.8	−6.68	−50.63	33.98
11e	15.7	−6.56	−54.09	33.27
11f	28.6	−6.38	−51.68	34.76
11g	10.2	−6.42	−51.04	34.51
11h	21.6	−6.72	53.21	33.91
11i	20.5	−6.96	−37.04	40.51
11j	3.6	−7.07	−57.33	37.59
11k	20.6	−6.25	−27.69	38.82
11l	8.2	−6.72	−52.27	34.01
11m	7.9	−5.93	−18.61	51.50
12a	10.3	−6.61	−40.88	28.37
12b	8.7	−6.06	−34.94	27.47
12c	9.0	−5.39	−45.34	30.33
13a	>100	−6.18	−22.35	33.89
13b	>100	−5.86	−33.92	25.12
13c	35.8	−5.30	−14.30	25.75
13d	33.9	−6.07	−31.23	38.45
13e	53.97	−6.64	−40.44	33.75
13k	>100	−6.59	−50.27	37.93
13l	7.9	−5.69	−30.21	42.42
14a	>100	−5.80	17.19	33.73
14b	>100	−5.79	−25.02	33.26
14c	>100	−5.08	−39.29	33.31
14d	22.4	−6.53	−43.52	112.89
14e	45.4	−6.53	−34.32	110.71
14f	9.4	−5.27	−58.19	106.01
14h	5.6	−5.90	−41.38	108.68
14j	6.7	−6.74	−31.01	56.13
14k	18.5	−5.17	−51.81	40.27
14m	17.8	−5.46	−29.90	33.34
14n	44.7	−5.53	−16.55	33.14
15a	>100	−5.00	−23.92	33.82
15b	12.4	−4.78	−36.38	35.69
15c	8.4	−5.09	−51.29	99.72
15d	44.7	−5.12	−31.13	36.86
15e	49.6	−5.37	−22.72	37.17
16a	>100	−5.16	−35.39	42.30
16b	9.9	−4.74	−40.17	30.20
17c	>100	−5.44	−35.39	42.30
17d	50.3	−5.51	−33.73	41.62
17e	22.4	−5.61	−29.73	−29.73
18a	>100	−5.31	−25.81	47.42
18b	12.6	−6.21	25.38	34.38
19a	>100	−4.78	−26.63	47.42
19b	10.6	−5.64	−30.21	35.84
Hopeaphenol (control)	0.11	−9.60	−128.44	84.71

A, seven (i.e. **10h, 11j, 11l, 12c, 14f, 14h**, and **15c**) showed amongst the lowest ΔG_{bind} values of <40 kcal/mol. This is an indication that re-scoring the docked complexes using this method could provide better insights into the structure-activity relationship than the docking scores [45].

Structure-activity relationships

The structure-activity relationship studies for the target compounds revealed that the position and the nature of the substituent on both the phenyl ring of the isoquinoline moiety and the oxindole moiety affect the inhibitory potential of the compounds. For example, it was found that the presence of a bulky hydrophobic substituent such as the naphthyl group at the 1-position of the oxindole moiety was shown to be important for activity. Compounds devoid of this fragment were either only very moderately active or completely inactive. Also, the presence of a hydroxyl group attached to the phenyl ring of the isoquinoline fragment was shown to be vital for inhibitory activity, though this depends on the position of the hydroxyl group. For example, comparing the biological activity of compounds **10j** and **11j**, each containing a naphthyl group at the 1-position of the oxindole fragment and an OH group on the phenyl ring of the isoquinoline fragment. Compound **11j** with the OH group at the 6′-position on the phenyl ring of the isoquinoline fragment was shown to be two times more effective for spike/ACE2 inhibition than compound **10j** with the OH group at the 8′-position at the phenyl ring of the isoquinoline fragment. This could be explained by the possibility

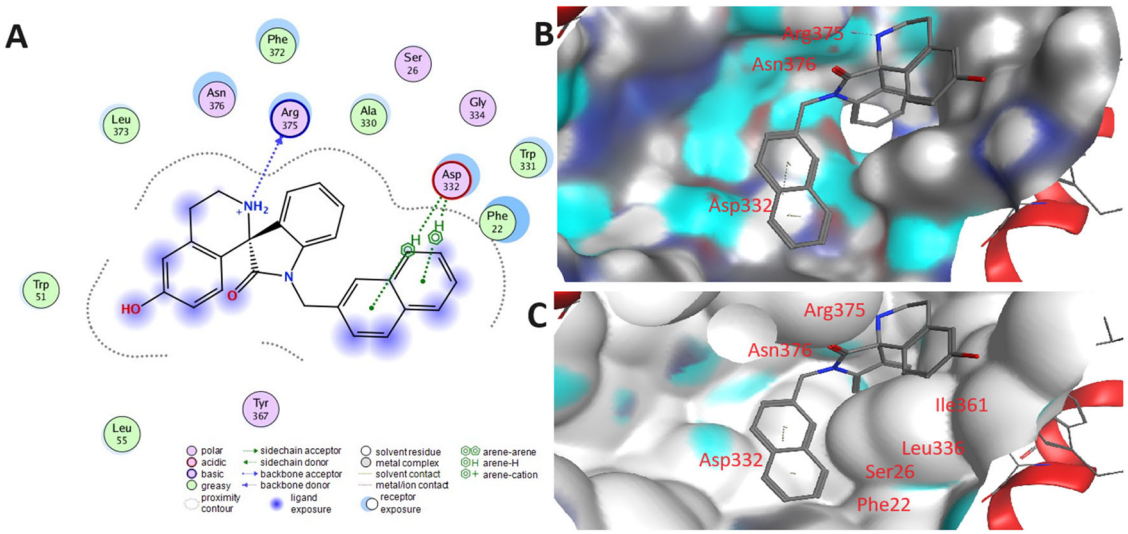

Fig. 2 Protein-ligand interactions of the most active of the synthesized spirooxindoles **11j**; **A** a 2D representation showing the H-bonding with Arg375 and Arene-H interactions with Asp332, **B** a 3D representation cast against the background of the molecular surface showing hydrophobic regions in grey, polar regions in blue and mildly polar regions in cyan, **C** a 3D representation cast against the background of the van der Waals surface highlighting the amino acid residues that form the hydrophobic patch

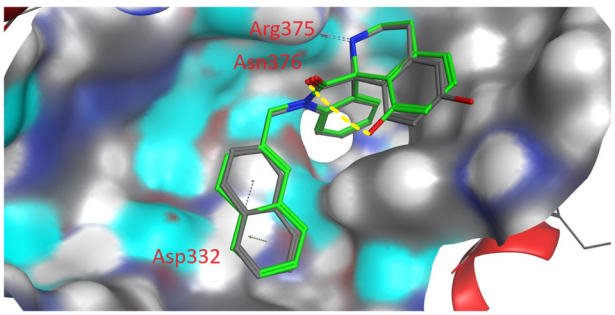

Fig. 3 A superposition of the isomers (compounds **10j** and **11j**) in the angiotensin II site, showing protein-ligand interactions with Arg375 and Asp332, with Asn376 in the background of the molecular surface. The color coding of the molecular surface is as in Fig. 2B, while intermolecular H-bonding is shown in grey broken lines and intramolecular H-bonding is shown in yellow broken lines. Both ligands are shown in stick representation and C-atoms of compound **10j** are shown in green, while those of compound **11j** are shown in grey

of intra-molecular H-bonding in **10j**, instead of intermolecular H-bonding with the protein (in the case of **11j**) Further investigation geared towards designing naphthyl-based analogs with hydrophobic substituents could help identify the most effective substitutions and positions that optimize the inhibitory capacity of these compounds.

Predicted DMPK profiles of active compounds

The initial prediction of drug metabolism and pharmacokinetics profiles of compounds would often help avoid attrition at later stages of the drug discovery process [46, 47]. A summary of the predicted parameters often related to drug metabolism and pharmacokinetics of the active compounds have been summarized in Table 2, while those of the moderately active compounds are shown in the Supplementary Material. The prediction of DMPK values of small molecules has been proven to help quickly identify compounds that will likely fail before clinical trials, thereby reducing the cost of identification of lead compounds [38, 39]. It was observed that, apart from two of the category A compounds (**14f** and **14h**) which showed 1 or 2 violations of Lipinski's rule of 5 (often related to drug bioavailability), the rest showed no violations. We also observed that eight of the active and moderately active compounds (**10f, 10h, 10j, 10l, 12a, 12b, 12c**, and **14m**) showed one PAINS alert, which is often characteristic of compounds that interfere in assays. However, only six of the compounds of category A showed this violation. None of the compounds violated Veber's rules related to bioavailability, whereas all violations against lead-likeness were ≤2. Besides, the majority of the active and moderately active compounds were predicted to show no blockage of human ether-a-go-go related gene (HERG) channels, renal toxicity, or hepatotoxicity. These parameters indicate that the compounds have promise towards further development against SARS-CoV-2.

Conclusion

To the best of our knowledge, this is the first report that shows that spirooxindoles have activity against SARS-

Table 2 Summary of the biological and physicochemical properties, drug-likeness filters, pharmacokinetic, and toxicity profiles of the active compounds

Ligands	MW (Da)[a]	log P[b]	NRB[c]	Lipinski Viol[d]	BBB[e]	Pgp[f]	Sol[g]	Log k_p[h]	PAINS[i]	HIA[j]	Bioavalability[k]	Veber[l]	Leadlikeness[m]
10f	435.32	4.09	2	0	0.16	Yes	−3.44	−2.74	1	93.63	0.55	0	2
10h	370.45	3.63	2	0	−0.04	Yes	−4.31	−2.75	1	96.88	0.55	0	2
10j	406.48	4.48	2	0	−0.09	Yes	−5.65	−2.74	1	96.57	0.55	0	2
10l	425.31	4.63	2	0	0.13	Yes	−3.45	−2.74	1	91.95	0.55	0	2
11j	406.48	4.48	2	0	−0.04	Yes	−4.63	−2.74	0	93.71	0.55		2
11l	392.40	3.60	2	0	−0.39	Yes	−3.33	−2.75	0	94.17	0.55	0	2
11m	388.44	3.7	2	0	−0.09	Yes	−3.47	−2.74	0	94.26	0.55	0	2
12b	316.74	2.09	0	0	−0.95	Yes	−2.98	−2.73	1	96.27	0.55	0	0
12c	440.09	2.96	0	0	−1.14	Yes	−2.90	−2.73	1	94.21	0.55	0	1
13l	346.33	2.32	2	0	−0.44	Yes	−3.01	−2.79	0	94.17	0.55	0	0
14f	514.82	4.02	4	1	−0.23	Yes	−3.78	−2.80	0	96.31	0.55	0	2
14h	637.16	5.92	4	2	−0.17	Yes	−4.08	−2.75	0	92.56	0.17	0	2
14j	432.49	4.087	4	0	−0.15	Yes	−3.78	−2.80	0	96.28	0.55	0	2
15c	468.14	3.57	2	0	−0.13	Yes	−3.11	−2.84	0	92.25	0.55	0	1
16b	369.37	2.29	3	0	−0.25	Yes	−3.70	−2.75	0	92.29	0.55	0	1
Ligands	VD_{ss}[n]	$Frac_{ub}$[o]	CNS[p]	CYP_{2D6}[q]	Cl_{tot}[r]	E_{Ren}[s]	Tox_{AMESs}[t]	D_{max}[u]	hERG I[v]	Tox_{ORA} (LD_{50})[w]	Tox_{Hep}[x]	$Tox_{T.p}$[y]	Tox_{Minnow}[z]
10f	0.61	0.17	−1.73	Yes	0.98	No	Yes	0.53	No	2.62	No	0.28	−0.22
10h	0.75	0.13	−1.76	No	0.99	No	Yes	0.15	Yes	3.12	Yes	0.35	0.83
10j	−0.07	0.22	−1.55	No	1.02	No	Yes	0.25	No	3.07	Yes	0.28	0.96
10l	0.65	0.17	−1.62	Yes	0.96	No	Yes	0.46	No	2.63	No	0.28	−0.57
11j	−0.03	0.18	−1.50	No	1.08	No	Yes	0.56	No	2.89	Yes	0.28	0.16
11l	0.68	0.15	−1.88	Yes	0.91	Yes	Yes	0.38	No	2.84	No	0.28	−0.32
11m	0.48	0.11	−1.79	Yes	0.99	Yes	Yes	0.5	No	2.48	Yes	0.28	0.43
12b	1.27	0.21	−2.308	No	1.09	No	No	0.26	No	1.84	Yes	0.29	1.19
12c	1.22	0.28	−2.13	No	0.72	No	No	0.07	No	2.40	Yes	0.28	0.52
13l	0.64	0.27	−2.40	No	1.01	No	No	−0.16	No	2.19	Yes	0.30	1.56
14f	0.92	0.16	−1.88	No	1.23	No	Yes	−0.274	Yes	3.17	Yes	0.28	−1.34
14h	0.76	0.11	−1.54	No	0.59	No	No	0.04	No	3.11	No	0.28	−1.69
14j	0.83	0.17	−1.89	No	1.01	No	Yes	−0.078	Yes	3.18	No	0.28	−0.68
15c	0.95	0.29	−2.03	No	0.71	No	No	−0.11	No	2.91	Yes	0.30	0.19
16b	0.93	0.19	−2.40	No	0.68	No	No	−0.05	No	3.77	Yes	0.37	−0.12

[a]Molecular weight in Daltons

[b]Logarithm of octanol/water partition coefficient

[c]Number of rotatable single bonds

[d]Number of Lipinski violations

[e]Numeric blood-brain barrier permeability (log BB)

[f]P-glycoprotein binding affinity

[g]Numeric water solubility (log mol/L)

[h]Logarithm of skin permeability in (cm/h)

[i]Number of pan-assay interference (PAINS) alerts predicted by SwissAdme

[j]Human intestinal absorption (% absorbed) predicted from pkCSM

[k]Abbott Bioavailability Score: Probability of F > 10% in rat (from SwissAdme)

[l]Passed the Veber (GSK) filter (Yes/No) predicted by SwissAdme

[m]Lead-likeness prediction

[n]Volume of distribution in human predicted by pkCSM in log L/kg

[o]Fraction of unbound drug (human) predicted by pkCSM in fractional unit

[p]Numeric predicted central nervous system permeability (from pkSCM)

[q]CYP2D6 inhibition by pkCSM (Yes/No)

[r]Total predicted rate of clearance by pkCSM in log ml/min/kg

[s]Renal excretion OCT2 substrate predicted by pkCSM (Yes/No)

[t]AMES toxicity prediction by pkCSM (Yes/No)

[u]Maximum tolerated dose in humans predicted by pkCSM in log mg/kg/day

[v]predicted hERG I inhibitor by pkCSM (Yes/No)

[w]predicted Oral Rat Acute Toxicity (LD_{50}) by pkCSM in mol/kg

[x]predicted pkCSM hepatotoxicity (Yes/No)

[y]*Tetrahymena pyriformis* fish species toxicity predicted by pkCSM in numeric (log μg/L)

[z]Minnow fish species toxicity predicted by pkCSM in numeric (log mM)

CoV-2 spike/ACE2 interaction. Five newly reported and fifty already published spirooxindoles [40–42], synthesized by Pictet-Spengler cyclodehydration, were screened against spike/ACE2 inhibition. It was shown that fifteen compounds had $IC_{50} < 10\,\mu M$ in the spike/ACE2 assay, while nine compounds were shown to be moderately active, and the rest were inactive. Molecular docking and evaluation of the structure-activity relationship showed that H-bonding between the isoquinoline moiety and the Arg375/Asn376 pair was required for activity. Besides, the presence of a bulky hydrophobic moiety attached to the oxindole is important for activity by potentially forming π-π stacking with Trp331, arene-H interactions with Asp332, and the strong hydrophobic interactions with the patch created by the amino acids Phe22, Ser26, Leu333, and Ile361. It would be necessary to further design new naphthyl-based analogs with hydrophobic substituents that address this region of the binding site to improve the activity against SARS-CoV-2 spike/ACE2 binding. Natural products have been shown to have promise for the development of new lead compounds for the discovery of SARS-CoV-2 drugs [48, 49]. In this work, we have been able to exploit the structures of the natural product fragments, tetrahydroisoquinoline and oxindole, as a molecular hybrid, to obtain a new set of SARS-CoV-2 spike/ACE2 blockers that have promise to prevent the transmission of the COVID-19 viral infection.

Experimental

General experimental procedure

Chemicals were purchased from Sigma-Aldrich Chemicals Company and were used as was supplied. All solvents were reagent grade. Where necessary, solvents and starting materials were purified using standard procedures. Solvent removal was carried out under reduced pressure using a Buchi rotary evaporator at temperatures not greater than 60°C. Melting points were measured using a Mel-Temp II apparatus with the use of open capillaries and were uncorrected. The progress of all reactions was monitored by thin layer chromatography (TLC) on aluminum-backed silica gel 60 F254 plates obtained from Sigma-Aldrich; visualization was by UV light at 254 nm or by staining with iodine. The compounds were purified by medium-pressure liquid chromatography over silica gel 60-to-400 mesh, using the appropriate solvent systems.

High-resolution Fourier transform mass spectrometry electrospray ionization (FTMS-ESI) mass spectra were generated using an LTQ Orbitrap XL mass spectrometer (Thermo Fisher Scientific, Bremen, Germany). A heated electrospray interface (H-ESI) was operated for ionization of the molecules at a spray voltage of 5 kV. Capillary voltage and tube lens voltages were then adjusted to 20 and 100 V, respectively. The vaporizer temperature was set at 250°C and the ion transfer capillary temperature was set to 200°C. Measurements were carried out in the positive ion mode in a mass range of m/z 100–600 at a mass resolution of 60 000 at m/z 200. MS/MS experiments were performed using argon as collision gas in collision-induced dissociation (CID) mode, with collision energies measured at 15, 25 and 35 eV.

Nuclear magnetic resonance (NMR) spectra were obtained using a Bruker Avance III spectrometer operating at 600 MHz (H1) and 150 MHz (^{13}C). Spectra were recorded in deuterated solvents and referenced to residual solvent signals. Chemical shifts (δ) were measured in parts per million. Hydrogen and carbon assignments were done using gradient correlation spectroscopy (gCOSY), gradient heteronuclear single quantum correlation (gHSQC) spectroscopy, and heteronuclear multiple bond correlation (gHMBC) techniques. Multiplicities are reported as singlet (s), doublet (d), doublet of doublets (dd), doublet of triplets (dt), triplet (t), triplet of doublets (td) and multiplet (m). Coupling constants (J) are reported in Hertz. For biological evaluation, all compounds were converted to the corresponding hydrochlorides by treatment of the free bases with methanolic HCl. All compounds are greater than 95% pure by high-performance liquid chromatography (HPLC) analysis.

Synthesis of additional spirooxindoles

*Synthesis of 5,7-dibromo-6′,7′-dihydroxy-3′,4′-dihydro-2′H-spiro[indoline-3,1′-isoquinolin]-2-one (**12c**) following Method A.*

The compound was synthesized via the phenolic Pictet–Spengler reaction, as reported [50]. To a solution of 5,7-dibromo isatin (1.5 g, 5.1 mmol) in absolute ethanol (10 ml) was added dopamine (1 g, 5.1 mmol) and triethylamine (1 ml). The reaction mixture was stirred and heated under reflux for 7–10 h, and subsequently concentrated under reduced pressure to remove the solvent. Distilled water was added to the resulting viscous mass and the product, which precipitated out was extracted into ethyl acetate (3 × 30 ml). The combined organic extracts were dried over anhydrous sodium sulfate and concentrated to a minimum volume. The crude product was further purified by column chromatography (hexane: ethyl acetate – 60:40). The final product was re-crystallized from absolute ethanol. Yield, 1.7 g, 76% (brown solid). M.p. 256–258°C (HCl salt).

^{1}H NMR (CD_3OD, 700 MHz): δ ppm 2.74 (dt, $J = 16.1$, 4.6 Hz, 1H, H4′a), 2.90 (ddd, $J = 15.9$, 5.4 Hz, 1H, H4′b), 3.10–3.15 (m, H3′a), 3.71–3.77 (m, H3′b), 5.91 (s, 1H, H8′), 6.62 (s, 1H, H5′), 7.27 (d, $J = 1.8$ Hz, 1H, H4), 7.64

(d, $J = 1.8$ Hz, 1H, H6). **^{13}C NMR** (CD_3OD, 175 MHz): δ ppm 27.2 (C4′), 38.4 (C3′), 64.7 (C3/C1′), 102.8 (C7), 111.9 (C8′), 114.9 (C5), 115.4 (C5′), 123.5 (C8′a), 126.7 (C4), 127.3 (C4′a), 133.6 (C6), 138.7 (C3a), 140.9 (C7a), 143.8 (C7′), 145.0 (C6′), 180.1 (C2). MS(ESI): cald for $C_{16}H_{12}Br_2N_2O_3$ $[M + H]^+$ 440.09, found 440.93; LC(ESI): t_R 8.77 min, purity 90%.

*General method for the synthesis of 6-methoxy- & 6′,7′-dimethoxy-3′,4′-dihydro-2′H-spiro[indoline-3,1′-isoquinolin]-2-ones (**13l &14h**) following Method B.*

A mixture of the appropriate isatin (1 equiv), methoxyphenethylamine (1.2 equiv), and polyphosphoric acid (2 g) was heated in an oil bath (bath temperature at 100°C) while stirring mechanically for 5 h. Upon completion of the reaction, as revealed by TLC, the reaction mixture was allowed to cool to about 50°C and quenched by slow addition of water. To this mixture, a saturated solution of sodium carbonate to adjust the pH to 11. The floating product obtained was extracted into ethyl acetate (3 × 30 ml). The combined organic extracts were dried over anhydrous sodium sulfate and concentrated under reduced pressure to obtain the crude product. The latter was purified using suitable solvent systems by flash chromatography on silica gel. Yields ranged between 60 and 98%.

*6′-methoxy-5-methyl-3′,4′-dihydro-2′H-spiro[indoline-3,1′-isoquinolin]-2-one (**13l**) following Method B*. This was prepared from 5-methylisatin (2.8 g, 17 mmol), 3-methoxyphenethylamine (2.6 g 17 mmol), and polyphosphoric acid (3 g). The crude product was purified by flash chromatography (hexane: ethyl acetate – 80:20). Yield, 4.6 g, 92% (brown solid), M.p. 208–209°C.

^{1}H NMR (DMSO-d_6, 600 MHz): δ ppm 1.46 (s, 3H, 5-C$\underline{H_3}$), 2.07 -2.13 (m, 1H, H4′a), 2.23 (ddd, $J = 16.5$, 8.7, 5.3 Hz, 1H, H4′b), 2.39 (dt, $J = 12.8$, 5.2 Hz, 1H, H3′a), 2.96 (d, $J = 5.1$ Hz, 4H, H3′b, m, 4H, 7′-OC$\underline{H_3}$), 5.64 (d, $J = 8.6$ Hz, 1H, H8′), 5.80 (dd, $J = 8.6$, 2.7 Hz, 1H, H7′), 5.95 (d, $J = 2.7$ Hz, 1H, H5′), 6.07 (d, $J = 7.87$ Hz, 1H, H7), 6.14–6.17 (m, 1H, H4), 6.29 (ddd, $J = 7.9$, 1.7, 0.8 Hz, 1H, H6). **^{13}C NMR** (DMSO-d_6, 150 MHz): δ ppm 18.9 (5-$\underline{C}H_3$), 27.6 (C4′), 37.5 (C3′), 53.4 (6′- O$\underline{C}H_3$), 62.9 (C3/C1′), 108.7 (C7), 111.8 (C7′), 112.6 (C5′), 124.3 (C4), 125.4 (C8′a), 126.4 (C8′), 128.3 (C6), 131.5 (C3a), 134.5 (C7a), 136.4 (C4′a), 138.4 (C5), 158.0 (C6′), 180.3 (C2). MS(ESI): cald for $C_{18}H_{18}N_2O_2$ $[M + H]^+$ 294.35, found 294.15; LC(ESI): t_R 9.52 min, purity 93%.

*1-(4-fluorobenzyl)-6′,7′-dimethoxy-5-methyl-3′,4′-dihydro-2′H-spiro[indoline-3,1′-isoquinolin]-2-one (**14h**) following Method B.*

This was prepared from 5-methyl-1-(4-fluorobenzyl) indoline-2,3-dione (1 g, 3.7 mmol), 3,4- dimethoxyphenethylamine (0.8 g, 4.4 mmol) and polyphosphoric acid (3 g). The crude product was purified by flash chromatography (hexane: ethyl acetate – 60:40). Yield, 1.4 g, 90% (brown solid), M.p. 99–101°C

^{1}H NMR (DMSO-d_6, 600 MHz): δ ppm 2.19 (s, 3H, 5-C$\underline{H_3}$), 2.71 (dt, $J = 15.9$, 4.1 Hz, 1H, H4′a), 2.88 (ddd, $J = 15.1$, 9.3, 5.4 Hz, 1H, H4′b), 3.05 (ddd, $J = 12.5$, 5.4, 4.1 Hz, 1H, H3′a), 3.29(s, 3H, 7′-OC$\underline{H_3}$), 3.65 (ddd, $J = 12.4$, 9.3, 4.3 Hz, 1H, H3′b), 3.74 (s, 3H, 6′-OC$\underline{H_3}$), 4.76 (d, $J = 15.6$ Hz, 1H, C$\underline{H_2}$-Ar), 4.96 (d, $J = 15.6$ Hz, 1H, C$\underline{H_2}$-Ar), 5.72 (s, 1H, H8′), 6.76 (s, 1H, H5′), 6.92 (dd, $J = 4.8$, 3.1 Hz, 2H, H4, H7), 7.05 (ddd, $J = 8.0$, 1.8, 0.9 Hz, 1H, H6), 7.16–7.18 (m, H3″, H5″), 7.42 (dd, $J = 8.6$, 5.5 Hz, 2H, H2″, H6″). **^{13}C NMR** (DMSO-d_6, 150 MHz): δ ppm 21.0 (5-$\underline{C}H_3$), 28.7 (C4′), 38.9 (C3′), 42.2 ($\underline{C}H_2$-Ar), 55.8 (7′-O$\underline{C}H_3$), 56.0 (6′-O$\underline{C}H_3$), 63.6 (C3/C1′), 109.2 (C7), 109.4 (C8′), 113.0 (C5′), 115.8 (C3″, C5″), 125.5 (C4), 127.2 (C8′a), 129.3 (C6), 129.5 (C4′a), 129.9 (C2″, C6″), 132.2 (C3a), 133.5 (C1″), 135.5 (C5), 140.4 (C7a), 148.5 (C7′), 148.5 (C6′), 161.2 (C4″), 178.8 (C2). MS(ESI): cald for $C_{26}H_{25}FN_2O_3$ $[M + H]^+$ 432.49, found 432.19; LC(ESI): t_R 17.50 min, purity 70%.

*Synthesis of N-ethyl-6′,7′-dimethoxy-1-(4-methylbenzyl)-2-oxo-3′,4′-dihydro-2′H-spiro[indoline-3,1′-isoquinoline]-2′-carboxamide (**17c**) following Method C.*

The target compound was prepared from the previously described 6′,7′-dimethoxy-1-(4-methylbenzyl)-3′,4′-dihydro-2′*H*-spiro[indoline-3,1′-isoquinolin]-2-one **14e** (1 g, 2.4 mmol) and ethyl isocyanate (0.21 g, 0.23 mL, 2.9 mmol, 1.2 eq). An acetonitrile solution of **14e** and ethyl isocyanate was heated to 60°C for 2 h. Upon completion of the reaction, the mixture was allowed to cool to room temperature, made basic by the slow addition of aqueous sodium bicarbonate to pH 10. The product was extracted into ethyl acetate (30 mL x 2), and the combined organic extracts were dried over anhydrous sodium sulfate and concentrated under reduced pressure. The crude product was purified by flash chromatography (hexane: ethyl acetate – 70:30). Yield, 0.6 g, 50% (white solid). M.p. 193–194°C.

^{1}H NMR (DMSO-d_6, 700 MHz): δ ppm 0.96 (t, $J = 7.17$ Hz, 3H, N1‴-$CH_2C\underline{H_3}$), 2.27 (s, 3H, 4″-C$\underline{H_3}$), 2.90 (ddd, $J = 15.4$, 4.8, 3.4 Hz, 1H, H4′a), 2.92 - 3.01 (m, 3H, 1H, H4′b, N1‴-C$\underline{H_2}$CH$_3$), 3.11 (s, 3H, 7′-OC$\underline{H_3}$), 3.55–3.60 (m, 1H, H3′a), 3.72 (s, 3H, 6′-OC$\underline{H_3}$), 3.97 (td, $J = 12.2$, 4.6 Hz, 1H, H3′b), 4.62 (d, $J = 15.5$ Hz, 1H, N1-C$\underline{H_2}$), 4.96 (d, $J = 15.5$ Hz, 1H, N1-C$\underline{H_2}$), 5.76 (s, 1H, H8′), 6.84 (s, 1H, H5′), 6.89 (td, $J = 7.5$, 1.0 Hz, 1H, H5), 6.93 (dt, $J = 7.9$, 0.7 Hz, 1H, H7), 7.03 (dd, $J = 7.3$, 1.25 Hz, 1H, H4), 7.10 - 7.13 (d, $J = 7.8$ Hz, 2H, H3″, H5″), 7.17 (td, $J = 7.7$, 1.3 Hz, 1H, H6), 7.31–7.34 (m, 2H, H2″, H6″). **^{13}C NMR** (DMSO-d_6, 175 MHz): δ ppm 15.8 (N1‴-$CH_2\underline{C}H_3$), 21.1 (4″-$\underline{C}H_3$), 30.0 (C4′), 35.4 (N1‴-$\underline{C}H_2CH_3$), 42.2 (C3′), 43.4 (N1-$\underline{C}H_2$), 55.4 (7′-O$\underline{C}H_3$), 55.9 (6′-O$\underline{C}H_3$), 65.5 (C3/C1′), 108.9 (C7), 109.1 (C8′), 112.3 (C5′), 122.3 (C4), 122.7 (C5), 126.5 (C8′a), 128.2 (C4′a), 128.3 (2C, C2″,

C6″), 128.9 (C6), 129.5 (2C, C3″, C5″), 134.5 (C1″), 135.7 (C3a)137.0 (C4″), 143.5 (C7a), 147.7 (C7′), 148.3 (C6′), 156.7 (C2‴), 177.3 (C2). MS(ESI): cald for $C_{29}H_{31}N_3O_4$ $[M + H]^+$ 485.57, found 485.24; LC(ESI): t_R 22.58 min, purity 95%.

*Synthesis 6′,7′-dimethoxy-2′-methyl-1-(4-methylbenzyl)-3′,4′-dihydro-2′H-spiro[indoline-3,1′-isoquinolin]-2-one (**17d**) following Method C.*

This compound was prepared from previously synthesized 6′,7′-dimethoxy-1-(4-methylbenzyl)-3′,4′-dihydro-2′*H*-spiro[indoline-3,1′-isoquinolin]-2-one (**14e**) [43] (1 g, 2.4 mmol) and formaldehyde (0.3 mL of 37% formalin, 3.6 mmol, 1.5 eq). To a formic acid solution of **14e** formaldehyde was added dropwise. The resulting mixture was heated at 60°C for 3 h, allowed to cool to room temperature, and made basic by slowly adding 2 M aqueous sodium hydroxide. The product was extracted into ethyl acetate (30 mL x 3), and the combined organic extracts were dried over anhydrous sodium sulfate and concentrated under reduced pressure. The crude product was purified by flash chromatography (hexane: ethyl acetate – 50:50). Yield, 0.8 g, 78% (yellow oil).

^{1}H NMR (DMSO-d_6, 700 MHz): δ ppm 2.06 (s, 3H, N2′-C$\underline{H}_3$), 2.26 (s, 3H, 4″-C$\underline{H}_3$), 2.78 (dt, $J = 15.8$, 3.6 Hz, 1H, H4′a), 2.88 (ddd, $J = 11.3$, 5.7, 2.9 Hz, 1H, H3′a), 3.03 (ddd, $J = 16.0$, 10.5, 5.6 Hz, 1H, 1H, H4′b), 3.22 (s, 3H, 7′-OC$\underline{H}_3$), 3.63 (td, $J = 10.9$, 4.1 Hz, 1H, H3′b), 3.73 (s, 3H, 6′-OC$\underline{H}_3$), 4.77 (d, $J = 15.4$ Hz, 1H, N1-C$\underline{H}_2$), 4.97 (d, $J = 15.5$ Hz, 1H, N1-C$\underline{H}_2$), 5.65 (s, 1H, H8′), 6.77 (s, 1H, H5′), 6.99–7.01 (m, 2H, H4, H5), 7.06 (d, $J = 7.9$ Hz, 1H, H7), 7.14 (d, $J = 7.8$ Hz, 2H, H3″, H5″), 7.26–7.29 (m, 3H, H6, H2″, H6″). **^{13}C NMR** (DMSO-d_6, 175 MHz): δ ppm 21.0 (4″-C$\underline{H}_3$), 28.7 (C4′), 39.6 (N2′-C$\underline{H}_3$), 42.7 (N1-C$\underline{H}_2$), 46.9 (C3′), 55.6 (7′-OC$\underline{H}_3$), 55.9 (6′-OC$\underline{H}_3$), 69.0 (C3/C1′), 109.6 (C8′), 109.6 (C7), 112.4 (C5′), 123.5 (C5), 124.8 (C4), 126.7 (C8′a), 128.0 (C4′a), 128.1 (2C, C2″, C6″), 129.4 (2C, C3″, C5″), 129.7 (C6), 133.2 (C3a), 134.2 (C1″), 137.3 (C4″), 143.5 (C7a), 147.4 (C7′), 148.5 (C6′), 177.3 (C2). MS(ESI): cald for $C_{27}H_{28}N_2O_3$ $[M + H]^+$ 428.52, found 428.21; LC(ESI): t_R 21.05 min, purity 90%.

Description of biological screening (AlphaScreen assay) procedure

SARS-CoV-2 spike-RBD binding to ACE2 was determined using AlphaScreen technology-based assay as described previously [51]. For RBD-ACE2 assays, 2 nM of ACE2-Fc (Sino Biological, Chesterbrook, PA, USA) was incubated with 5 nM HIS-tagged SARS-CoV-2 Spike-RBDs representing the parental USA-WA/2020 (“Wild-type” (WT)) sequence (SinoBiological) in the presence of 5 µg/mL nickel chelate donor bead in a total of 10 µL of 20 mM Tris (pH 7.4), 150 mM KCl, and 0.05% CHAPS. Test compounds were diluted to 100× final concentration in DMSO. 5 µL of ACE2-Fc/Protein A acceptor bead was first added to the reaction, followed by 100 nL test compound and then 5 µL of RBD-HIS/Nickel chelates donor beads. All conditions were performed in duplicate. Following incubation at room temperature for 2 h, luminescence signals were measured using a ClarioStar plate reader (BMC Labtech, Cary, NC, USA). Data were then normalized to percent inhibition, where 100% equaled the AlphaScreen signal in the absence of RBD-HIS, and 0% denoted the AlphaScreen signal in the presence of both protein and DMSO vehicle control.

Molecular modeling procedures

Target proteins for docking

Since the emergence of the COVID-19 pandemic, several computational methodologies have been employed in an attempt to identify lead compounds for drug discovery and development [52, 53] Molecular modeling protocols were performed, as previously reported [7–9, 51, 54, 55]. The docking evaluated protein-ligand interaction of the small molecules towards the ACE2 protein, as we had previously demonstrated that compounds that bind into the angiotensin II site of the ACE2 receptor would prevent recognition of the two proteins and, hence, binding of the viral to the ACE2 receptor [9, 55]. The protein structures (ID: 6M0J) for SARS-CoV-2 spike/ACE2, corresponding to the Wuhan strain were retrieved from the Protein Data Bank (PDB) [56–58] and used for the entire study.

Protein preparation

All water molecules were deleted using the Molecular Operating Environment (MOE) software [59]. The Protein Preparation Wizard integrated into the Schrödinger package software [60, 61] was used to prepare the protein by adding the missing hydrogen bonds, assigning bond orders, and filling the missing side chains using PRIME. After this, the protein structures were energy minimized to reduce atomic clashes and optimized their interactions with the ligands during docking. From the Schrödinger software, the commercialized Maestro package’s Epik-tool was used to predict the protonation states at a pH of 7.0 [62, 63]. Finally, a restrained energy minimization step was carried out using the Optimized Potentials for Liquid Simulations 2005 (OPLS2005) forcefield [64] on both proteins. During the protein optimization step, the root mean square deviation (RMSD) of the displacement of the atoms was set to end with the minimization at 0.3 Å.

Ligand preparation

The MOE [60] builder module was used to generate the 3D models of the library of synthesized spirooxindoles.

For consistency, only the *R* stereoisomers were prepared for docking, as these addressed the voluminous hydrophobic regions in the ACE2 site more appropriately during trial docking. The generated 3D structures were then energy minimized using the MMFF94 force field [65–71]. The ligands were further prepared for docking using the LigPrep tool to generate all the plausible tautomers of each ligand as implemented in Schrödinger's Maestro software package [63]. Using the incorporated OPLS2005 force field [64], the spirooxindole 3D structure library was further energy minimized. The ConfGen tool (implemented in the Schrödinger package) was then used to compute 60 conformers per ligand in the 3D library, by setting all other options to default except for the minimization of the output [60].

Docking and scoring

Docking was carried out using the Glide program incorporated in the Maestro package distributed by Schrödinger [61, 62] as shown in our recent publications [7–9, 51–55], with some modifications. Docking validation results on this protein have already been reported in our previously reported studies [57–59]. After the protein preparation phase, a docking grid box was generated for the spike/ACE2 complex to investigate how the ligands will bind around the following amino acid residues; Asp597, Thr598, Lys516, Val321, Gln121, Lys578, Ala283, Ser91, Asn746, Gln68, Pro744, Glu518 and Thr610. The ligand size for each of these grid boxes, which is the area where all the generated 3D structures were docked, was set to a maximum ligand size of 36 Å. While writing 10 poses per ligand conformer, 20 poses were included for each ligand conformer, and taking into consideration the input of ring conformation, all other settings were allowed to default. The outputs were scored using standard precision (SP) GlideScore as the scoring function [72].

Selection of binding modes

After the extraction of the results and the computation of carefully selected descriptors, the specific area ligands bound with the protein in the receptor binding domain (RBD) of both the Spike/ACE2, the binding modes, and the residues taking part in the interaction during binding were observed using MOE [60]. Browsing through the docking results and establishing the ligand interactions of each docked protein-ligand complex made it possible to establish structure-activity relationships (SAR) in the RBD in both cases and to identify some ligand moieties important for activity and selectivity. The ligands in both protein RBD were then superimposed to highlight their preferred binding modes.

Re-scoring of docked poses by MM-GBSA

To properly explain the observed biological activities, the Molecular Mechanics Generalized Born Solvation Area (MM-GBSA) model was employed as a means of re-scoring the docked protein-ligand poses. The PRIME tool incorporated in the Maestro package from Schrödinger (2017) was used to do this [61]. The free energy of the binding (ΔG_{bind}) for each ligand towards the spike/ACE2 complex was calculated by using the Prime MM-GBSA algorithm (using default parameters). Each docked pose was retrieved from the Glide docking output and input on the PRIME program for calculating several thermodynamic properties including the binding free energy (ΔG_{bind}) and solvation free energy (ΔG_{solv}) values in kcal/mol. The binding pose of the complex structures was visually inspected by using the ligand interaction tool in MOE to gain insight into the binding mode (see additional notes on this method under Fig. S3, Supplementary Data).

Prediction of pharmacokinetic properties of the active compounds

An initial assessment of the risk of further developing the active molecules into lead compounds for the discovery of next-generation antiviral agents was conducted by prediction of the drug metabolism and pharmacokinetics properties of the active and moderately active compounds. The pharmacokinetic properties were conducted by the computation of parameters related to drug absorption, distribution, metabolism, and elimination by using the SwissADME web server [73]. Each chemical structure was converted to a simple molecular input line entry system (SMILES) and uploaded onto the SwissADME web server platform (http://www.swissadme.ch) [73]. This then enabled the computation of 46 descriptors often used to predict the DMPK (drug metabolism and pharmacokinetic) profiles. The computed descriptors were, amongst others, molecular weight, molar refractivity, number of rotatable bonds, Lipinski violations, aqueous solubility, Veber violations, Ghose violations, Egan violations, gastro-intestinal absorption, blood-brain-barrier permeability, cytochrome inhibition, synthetic accessibility, P-glycoprotein binding, skin permeability, Bioavailability score, Muegge violations, PAINS alerts, Lead-likeness violations, etc. Additional DMPK- and toxicity-related parameters were computed using the pkCSM web server (https://biosig.lab.uq.edu.au/pkcsm/) [74]. The pkCSM signatures are then applied across different pharmacokinetic properties to develop predictive regression and classification models to predict absorption, distribution, metabolism, excretion, and toxicity (ADMET). The additional parameters include

the steady-state volume of distribution, central nervous system (CNS) permeability, blood−brain barrier permeability, total clearance, and toxicity parameters like maximum recommended tolerated dose (MRTD), oral rat acute toxicity (LD_{50}), oral rat chronic, lowest observed adverse effect (LOAEL), as well as toxicity against fish species *Tetrahymena pyriformis* and fathead minnow toxicity (LC_{50}).

Data availability

No datasets were generated or analysed during the current study.

Supplementary information The online version contains supplementary material available at https://doi.org/10.1007/s00044-025-03386-5.

Acknowledgements We acknowledge the technical support of Mr. Cyril T. Namba-Nzanguim. A previous version of this manuscript had been submitted as a preprint through Researchsquare (https://www.researchsquare.com/article/rs-4535655/v1).

Author contributions Albert Enama Ehinak: Conceptualization, Methodology, Data curation, Formal analysis, Investigation, Writing – original draft. Maloba M.M. Lobe: Conceptualization, Methodology, Data curation, Formal analysis, Investigation, Writing – original draft. Donatus Bekindaka Eni: Methodology, Data curation, Formal analysis, Investigation, Conrad V. Simoben: Conceptualization, Formal analysis, Writing – review & editing, Ian Tietjen: Conceptualization, Funding acquisition, Investigation, Methodology, Writing – review & editing, Mathieu Jules Mbenga Tjegbe: Methodology, Data curation, Formal analysis, Investigation, Joel Cassel: Conceptualization, Investigation, Methodology, Writing – review & editing. Joseph M. Salvino: Funding acquisition, Investigation, Methodology, Supervision, Writing – review & editing. Luis J. Montaner: Funding acquisition, Investigation, Methodology, Supervision, Writing – review & editing. Wolfgang Sippl: Conceptualization, Formal analysis, Supervision, Writing – review & editing. Simon M. N. Efange: Conceptualization, Formal analysis, Supervision, Writing – review & editing. Fidele Ntie-Kang: Funding acquisition, Investigation, Methodology, Supervision, Writing – original draft, Writing – review & editing. All authors reviewed the manuscript.

Funding We acknowledge financial support from the Bill & Melinda Gates Foundation through the Calestous Juma Science Leadership Fellowship awarded to Fidele Ntie-Kang (grant award number: INV-036848 to University of Buea). FNK also acknowledges joint funding from the Bill & Melinda Gates Foundation and LifeArc (award number: INV-055897 and Grant ID: 10646) under the African Drug Discovery Accelerator program. FNK acknowledges further funding from the Alexander von Humboldt Foundation for a Research Group Linkage project (award number Ref [3].4- 1156361-CMR-IP). Open Access funding enabled and organized by Projekt DEAL.

Compliance with ethical standards

Conflict of interest The authors declare no competing interests.

Publisher's note Springer Nature remains neutral with regard to jurisdictional claims in published maps and institutional affiliations.

References

1. Pinto GP, Vavra O, Marques SM, Filipovic J, Bednar D, Damborsky J. Screening of world approved drugs against highly dynamical spike glycoprotein of SARS-CoV-2 using CaverDock and machine learning. Comput Struct Biotechnol J. 2021;19:3187–97. https://doi.org/10.1016/j.csbj.2021.05.043
2. World Health Organization, COVID-19 epidemiological update, 17 September 2024; https://www.who.int/europe/emergencies/situations/covid-19 (Accessed on 03 October 2024)
3. Ju SP, Yang YC, Chen HY. Unraveling the binding mechanisms of SARS-CoV-2 variants through molecular simulations. Heliyon. 2024;10:e27193. https://doi.org/10.1016/j.heliyon.2024.e27193
4. Wrobel AG. Mechanism and evolution of human ACE2 binding by SARS-CoV-2 spike. Curr Opin Struct Biol. 2023;81:102619. https://doi.org/10.1016/j.sbi.2023.102619
5. Jena NR. Drug targets, mechanisms of drug action, and therapeutics against SARS-CoV-2. Chem Phys Impact. 2021;2:100011. https://doi.org/10.1016/j.chphi.2021.100011
6. Adamson CS, Chibale K, Goss RJM, Jaspars M, Newman DJ, Dorrington RA. Antiviral drug discovery: preparing for the next pandemic. Chem Soc Rev. 2021;50:3647–55. https://doi.org/10.1039/d0cs01118e
7. Eni DB, Cassel J, Namba-Nzanguim CT, Simoben CV, Tietjen I, Akunuri R, et al. Design, synthesis, and biochemical and computational screening of novel oxindole derivatives as inhibitors of Aurora A kinase and SARS-CoV-2 spike/host ACE2 interaction. Med Chem Res. 2024;33:620–34. https://doi.org/10.1007/s00044-024-03201-7
8. Majoumo-Mbe F, Sangbong NA, Tadjong Tcho A, Namba-Nzanguim CT, Simoben CV, Eni DB, et al. 5-chloro-3-(2-(2,4-dinitrophenyl) hydrazono)indolin-2-one: synthesis, characterization, biochemical and computational screening against SARS-CoV-2. Chem Pap. 2024;78:3431–41. https://doi.org/10.1007/s11696-023-03274-5
9. Shu VA, Eni DB, Tjegbe MJM, Tietjen I, Cassel J, Salvino J, et al. Computer-aided design, synthesis, and biological evaluation of 4-chloro-N-(2-oxo-3-(2-pyridin-4-yl)hydrazineylidene)indolin-5yl) benzamide and1-(4-bromobenzyl)-5-indoline-2,3-dione against SARS-CoV-2 spike/ACE2. Microbe. 2024;4:100143. https://doi.org/10.1016/j.microb.2024.100143
10. Shu VA, Eni DB, Ntie-Kang F. A survey of isatin hybrids and their biological properties. Mol Divers. 2024. https://doi.org/10.1007/s11030-024-10883-z
11. Bedding MJ, Franck C, Johansen-Leete J, Aggarwal A, Maxwell JWC, Patel K, et al. Discovery of high affinity cyclic peptide ligands for human ACE2 with SARS-CoV-2 entry inhibitory activity. ACS Chem Biol. 2024;19:141–52. https://doi.org/10.1021/acschembio.3c00568
12. Loi LK, Yang CC, Lin YC, Su YF, Juan YC, Chen YH, et al. Decoy peptides effectively inhibit the binding of SARS-CoV-2 to

ACE2 on oral epithelial cells. Heliyon. 2023;9:e22614. https://doi.org/10.1016/j.heliyon.2023.e22614
13. Fraternale A, De Angelis M, De Santis R, Amatore D, Masini S, Monittola F, et al. Targeting SARS-CoV-2 by synthetic dual-acting thiol compounds that inhibit Spike/ACE2 interaction and viral protein production. FASEB J. 2023;37:e22741. https://doi.org/10.1096/fj.202201157RR
14. Papp H, Tóth E, Bóvári-Biri J, Bánfai K, Juhász P, Mahdi M, et al. The PARP inhibitor rucaparib blocks SARS-CoV-2 virus binding to cells and the immune reaction in models of COVID-19. Br J Pharmacol. 2024;181:4782–803. https://doi.org/10.1111/bph.17305
15. Emam MH, Mahmoud MI, El-Guendy N, Loutfy SA. Establishment of in-house assay for screening of anti-SARS-CoV-2 protein inhibitors. AMB Express. 2024;14:104. https://doi.org/10.1186/s13568-024-01739-8
16. Rosal RJZ, Paderes MC. Inhibiting SARS-CoV-2 viral entry by targeting spike:ACE2 interaction with *O*-modified quercetin derivatives. RSC Med Chem. 2024;15:3212–22. https://doi.org/10.1039/d4md00286e
17. Kim JY, Kim TY, Son SR, Kim SY, Kwon J, Kwon HC, et al. Triterpenoidal saponins from the leaves of *Aster koraiensis* offer inhibitory activities against SARS-CoV-2. Plants. 2024;13:303. https://doi.org/10.3390/plants13020303
18. Queirós-Reis L, Mesquita JR, Brancale A, Bassetto M. Exploring the fatty acid binding pocket in the SARS-CoV-2 spike protein - confirmed and potential ligands. J Chem Inf Model. 2023;63:7282–98. https://doi.org/10.1021/acs.jcim.3c00803
19. Dabrell SN, Li YC, Yamaguchi H, Chen HF, Hung MC. Herbal compounds dauricine and isoliensinine impede SARS-CoV-2 viral entry. Biomedicines. 2023;11:2914. https://doi.org/10.3390/biomedicines11112914
20. Pan B, Fang S, Wang L, Pan Z, Li M, Liu L. Quercetin: a promising drug candidate against the potential SARS-CoV-2-Spike mutants with high viral infectivity. Comput Struct Biotechnol J. 2023;21:5092–8. https://doi.org/10.1016/j.csbj.2023.10.029
21. Jancy SV, Lupitha SS, Chandrasekharan A, Varadarajan SN, Nelson-Sathi S, Prasad R, et al. A high-throughput screening system for SARS-CoV-2 entry inhibition, syncytia formation and cell toxicity. Biol Proced Online. 2023;25:22. https://doi.org/10.1186/s12575-023-00214-1
22. El-Kalyoubi SA, Ragab A, Abu Ali OA, Ammar YA, Seadawy MG, Ahmed A, et al. One-pot synthesis and molecular modeling studies of new bioactive spiro-oxindoles based on uracil derivatives as SARS-CoV-2 inhibitors targeting RNA polymerase and spike glycoprotein. Pharmaceuticals. 2022;15:376. https://doi.org/10.3390/ph15030376
23. Girgis AS, Panda SS, Srour AM, Abdelnaser A, Nasr S, Moatasim Y, et al. 3-Alkenyl-2-oxindoles: synthesis, antiproliferative and antiviral properties against SARS-CoV-2. Bioorg Chem. 2021;114:105131. https://doi.org/10.1016/j.bioorg.2021.105131
24. Lima CM, Freitas LH, Moraes CB, Barbosa CG, Opatz T, Victor MM. Synthesis of isatins and oxindoles derivatives as SARS-CoV-2 inhibitors evaluated through phenotypic screening with Vero cells. J Braz Chem Soc. 2023;34:745–53. https://doi.org/10.21577/0103-5053.20220138
25. Alzyoud L, Mahgoub RE, Mohamed FE, Ali BR, Ferreira J, Rabeh WM, et al. The discovery of novel small oxindole-based inhibitors targeting the SARS-CoV-2 main protease (M^{pro}). Chem Biodiv. 2023;20:e202301176. https://doi.org/10.1002/cbdv.202301176
26. Shah VR, Bhaliya JD, Patel GM. In silico approach: docking study of oxindole derivatives against the main protease of COVID-19 and its comparison with existing therapeutic agents. J Basic Clin Physiol Pharmacol. 2021;32:197–214. https://doi.org/10.1515/jbcpp-2020-0262
27. Barakat A, Mostafa A, Ali M, Al-Majid AM, Domingo LR, Kutkat O, et al. Design, synthesis and in vitro evaluation of spirooxindole-based phenylsulfonyl moiety as a candidate anti-SAR-CoV-2 and MERS-CoV-2 with the Implementation of combination studies. Int J Mol Sci. 2022;23:11861. https://doi.org/10.3390/ijms231911861
28. Girgis AS, Panda SS, Kariuki BM, Bekheit MS, Barghash RF, Aboshouk DR. Indole-based compounds as potential drug candidates for SARS-CoV-2. Molecules. 2023;28:6603. https://doi.org/10.3390/molecules28186603
29. Fawazy NG, Panda SS, Mostafa A, Kariuki BM, Bekheit MS, Moatasim Y, et al. Development of spiro-3-indolin-2-one containing compounds of antiproliferative and anti-SARS-CoV-2 properties. Sci Rep. 2022;12:13880. https://doi.org/10.1038/s41598-022-17883-9
30. Kikuchi AK, Chan SW, Mailem RC, Gomez MC, Tayo LL. In silico investigation of oxindole alkaloids from *Uncaria perrottetii* and *Uncaria lanosa* f. *philippinensis* for COVID-19 therapy: binding site prediction and molecular docking. In *Proceedings of the 12th International Conference on Biomedical Engineering and Technology*, 2022. Apr 20 (pp. 5–8)
31. Tran QT, Lee RC, Liu HJ, Ran D, Low VZ, To DQ, et al. Discovery and development of labdane-oxindole hybrids as small-molecule inhibitors against chikungunya virus infection. Eur J Med Chem. 2022;230:114110. https://doi.org/10.1016/j.ejmech.2022.114110
32. Liu J, Cao R, Xu M, Wang X, Zhang H, Hu H, et al. Hydroxychloroquine, a less toxic derivative of chloroquine, is effective in inhibiting SARS-CoV-2 infection in vitro. Cell Discov. 2020;6:16. https://doi.org/10.1038/s41421-020-0156-0
33. Yao X, Ye F, Zhang M, Cui C, Huang B, Niu P, et al. In vitro antiviral activity and projection of optimized dosing design of hydroxychloroquine for the treatment of severe acute respiratory syndrome coronavirus 2 (SARS-CoV-2). Clin Infect Dis. 2020;71:732–9. https://doi.org/10.1093/cid/ciaa237
34. Sturrock BRH, Chevassut TJT. Chloroquine and COVID-19 – a potential game changer? Clin Med. 2020;20:278–81. https://doi.org/10.7861/clinmed.2020-0129
35. Pastick KA, Okafor EC, Wang F, Lofgren SM, Skipper CP, Nicol MR, et al. Review: hydroxychloroquine and chloroquine for treatment of SARS-CoV-2 (COVID-19). Open Forum Infect Dis. 2020;7:ofaa130. https://doi.org/10.1093/ofid/ofaa130
36. Vincent MJ, Bergeron E, Benjannet S, Erickson BR, Rollin PE, Ksiazek TG, et al. Chloroquine is a potent inhibitor of SARS coronavirus infection and spread. Virol J. 2005;2:69. https://doi.org/10.1186/1743-422X-2-69
37. Gasmi A, Peana M, Noor S, Lysiuk R, Menzel A, Benahmed AG, et al. Chloroquine and hydroxychloroquine in the treatment of COVID-19: the never-ending story. Appl Microbiol Biotechnol. 2021;105:1333–43. https://doi.org/10.1007/s00253-021-11094-4
38. Tripathy S, Dassarma B, Roy S, Chabalala H, Matsabisa MG. A review on possible modes of action of chloroquine/hydroxychloroquine: repurposing against SAR-CoV-2 (COVID-19) pandemic. Int J Antimicrob Agents. 2020;56:106028. https://doi.org/10.1016/j.ijantimicag.2020.106028
39. Mailem RC, Chan SW, Kikuchi AK, Gomez MC, Tayo LL. In silico investigation of oxindole alkaloids from *Uncaria perrottetii* and *Uncaria lanosa* f. *philippinensis* for COVID-19 therapy: a ligand affinity and characterization study. In *Proceedings of the 12th International Conference on Biomedical Engineering and Technology*, 2022 Apr 20 (pp. 21–25)
40. Lobe MMM, Efange SMN. 3′,4′-Dihydro-2′H-spiro[indolin-3:1′-isoquinolin]-2-ones as potential anticancer agents: synthesis and preliminary screening. R Soc Open Sci. 2020;7:191316. https://doi.org/10.1098/rsos.191316

41. Efange NM, Lobe MMM, Keumoe R, Ayong L, Efange SMN. Spirofused tetrahydroisoquinoline-oxindole hybrids as a novel class of fast acting antimalarial agents with multiple modes of action. Sci Rep. 2020;10:17932. https://doi.org/10.1038/s41598-020-74824-0
42. Efange NM, Lobe MMM, Yamthe LRT, Pekam JNM, Tarkang PA, Ayong L, et al. Spirofused tetrahydroisoquinoline-oxindole hybrids (spiroquindolones) as potential multitarget antimalarial agents: preliminary hit optimization and efficacy evaluation in mice. Antimicrob Agents Chemother. 2022;66:e0060722. https://doi.org/10.1128/aac.00607-22
43. Ruatta SM, Prada Gori DN, Fló Díaz M, Lorenzelli F, Perelmuter K, Alberca LN, et al. Garbage in, garbage out: how reliable training data improved a virtual screening approach against SARS-CoV-2 M^{pro}. Front Pharmacol. 2023;14:1193282. https://doi.org/10.3389/fphar.2023.1193282
44. Chen YC. Beware of docking! Trends Pharmacol Sci. 2015;36:78–95. https://doi.org/10.1016/j.tips.2014.12.001
45. Ntie-Kang F, Kannan S, Wichapong K, Owono Owono LC, Sippl W, Megnassan E. Binding of pyrazole-based inhibitors to *Mycobacterium tuberculosis* pantothenate synthetase: docking and MM-GB(PB)SA analysis. Mol Biosyst. 2014;10:223–39. https://doi.org/10.1039/c3mb70449a
46. Onguéné PA, Simoben CV, Fotso GW, Andrae-Marobela K, Khalid SA, Ngadjui BT, et al. In silico toxicity profiling of natural product compound libraries from African flora with anti-malarial and anti-HIV properties. Comput Biol Chem. 2018;72:136–49. https://doi.org/10.1016/j.compbiolchem.2017.12.002
47. Ntie-Kang F, Lifongo LL, Judson PN, Sippl W, Efange SM. How "drug-like" are naturally occurring anti-cancer compounds? J Mol Model. 2014;20:2069. https://doi.org/10.1007/s00894-014-2069-z
48. Singla RK, De R, Efferth T, Mezzetti B, Sahab Uddin M, Sanusi, et al. The International Natural Product Sciences Taskforce (INPST) and the power of Twitter networking exemplified through #INPST hashtag analysis. Phytomedicine. 2023;108:1545203. https://doi.org/10.1016/j.phymed.2022.154520
49. Ebob OT, Babiaka SB, Ntie-Kang F. Natural products as potential lead compounds for drug discovery against SARS-CoV-2. Nat Prod Bioprospect. 2021;11:611–28. https://doi.org/10.1007/s13659-021-00317-w
50. Ngo Hanna J, Ntie-Kang F, Kaiser M, Brun R, Efange SMN. 1-Aryl-1,2,3,4- tetrahydroisoquinolines as potential antimalarials: synthesis, in vitro antiplasmodial activity and in silico pharmacokinetics evaluation. RSC Adv. 2014;4:22856–65. https://doi.org/10.1039/C3RA46791K
51. Tietjen I, Cassel J, Register ET, Zhou XY, Messick TE, Keeney F, et al. The natural stilbenoid (-)-hopeaphenol inhibits cellular entry of SARS-CoV-2 USA-WA1/2020, B.1.1.7, and B.1.351 variants. Antimicrob Agents Chemother. 2021;65:e00772213. https://doi.org/10.1128/AAC.00772-21
52. Hasan AH, Hussen NH, Shakya S, Jamalis J, Pratama MRF, Chander S, et al. In silico discovery of multi-targeting inhibitors for the COVID-19 treatment by molecular docking, molecular dynamics simulation studies, and ADMET predictions. Struct Chem. 2022;33:1645–65. https://doi.org/10.1007/s11224-022-01996-y
53. Salih RHH, Hasan AH, Hussein AJ, Samad MK, Shakya S, Jamalis J, et al. One-pot synthesis, molecular docking, ADMET, and DFT studies of novel pyrazolines as promising SARS-CoV-2 main protease inhibitors. Res Chem Intermed. 2022;48:4729–51. https://doi.org/10.1007/s11164-022-04831-5
54. Simoben CV, Ghazy E, Zeyen P, Darwish S, Schmidt M, Romier C, et al. Binding Free Energy (BFE) Calculations and quantitative structure-activity relationship (QSAR) analysis of *Schistosoma mansoni* histone deacetylase 8 (smHDAC8) inhibitors. Molecules. 2021;26:25843. https://doi.org/10.3390/molecules26092584
55. Divsalar DN, Simoben CV, Schonhofer C, Richard K, Sippl W, Ntie-Kang F, et al. Novel Histone deacetylase inhibitors and HIV-1 latency-reversing agents identified by large-scale virtual screening. Front Pharmacol. 2020;11:905. https://doi.org/10.3389/fphar.2020.0090
56. Namba-Nzanguim CT, Simoben CV, Bekono BD, Tietjen I, Cassel J, Salvino JM, et al. Investigation of some plant stilbenoids and their fragments for the identification of inhibitors of SARS-CoV-2 viral spike/ACE2 protein binding. Microbe. 2024;3:1000593. https://doi.org/10.1016/j.microb.2024.100059
57. Berman HM, Westbrook J, Feng Z, Gilliland G, Bhat TN, Weissig H, et al. The protein data bank. Nucleic Acids Res. 2000;28:235–42. https://doi.org/10.1093/nar/28.1.235
58. Burley SK, Berman HM, Christie C, Duarte JM, Feng Z, Westbrook J, et al. RCSB Protein Data Bank: sustaining a living digital data resource that enables breakthroughs in scientific research and biomedical education. Protein Sci. 2018;27:316–30. https://doi.org/10.1002/pro.3331
59. Burley SK, Berman HM, Kleywegt GJ, Markley JL, Nakamura H, Velankar S. Protein Data Bank (PDB): the single global macromolecular structure archive. Methods Mol Biol. 2017;1607:627–41. https://doi.org/10.1007/978-1-4939-7000-1_26
60. Chemical Computing Group, Molecular, Operating Environment (MOE), version 2016.08, 2016
61. Schrödinger E. Release 2017-2. New York, NY, USA: Maestro, S.; LLC; 2017.
62. Sastry GM, Adzhigirey M, Day T, Annabhimoju R, Sherman W. Protein and ligand preparation: parameters, protocols, and influence on virtual screening enrichments. J Comput Aided Mol Des. 2013;27:221–34. https://doi.org/10.1007/s10822-013-9644-8
63. Shelley JC, Cholleti A, Frye LL, Greenwood JR, Timlin MR, Uchimaya M. Epik: a software program for pK_a prediction and protonation state generation for drug-like molecules. J Comput Aided Mol Des. 2007;21:681–91. https://doi.org/10.1007/s10822-007-9133-z
64. Banks JL, Beard HS, Cao Y, Cho AE, Damm W, Farid R, et al. Integrated Modeling Program, Applied Chemical Theory (IMPACT). J Comput Chem. 2005;26:1752–80. https://doi.org/10.1002/jcc.20292
65. Halgren TA. Merck molecular force field. I. Basis, form, scope, parameterization, and performance of MMFF94. J Comput Chem. 1996;17:490–519. https://doi.org/10.1002/(SICI)1096-987X(199604)17:5/6
66. Halgren TA. Merck molecular force field. II. MMFF94 van der Waals and electrostatic parameters for intermolecular interactions. J Comput Chem. 1996;17:520–52. https://doi.org/10.1002/(SICI)1096-987X(199604)17:5/6
67. Halgren TA. Merck molecular force field. III. Molecular geometries and vibrational frequencies for MMFF94. J Comput Chem. 1996;17:553–86. https://doi.org/10.1002/(SICI)1096-987X(199604)17:5/6
68. Halgren TA, Nachbar RB. Merck molecular force field. IV. Conformational energies and geometries for MMFF94. J Comput Chem. 1996;17:587–615. https://doi.org/10.1002/(SICI)1096-987X(199604)17:5/6
69. Halgren TA. Merck molecular force field. V. Extension of MMFF94 using experimental data, additional computational data, and empirical rules. J Comput Chem. 1996;17:616–41. https://doi.org/10.1002/(SICI)1096-987X(199604)17:5/6
70. Shawn Watts K, Dalal P, Murphy RB, Sherman W, Friesner RA, Shelley JC. ConfGen: a conformational search method for efficient generation of bioactive conformers. J Chem Inf Model. 2010;50:534–46. https://doi.org/10.1021/ci100015j

71. Ibezim A, Onuku RS, Ibezim A, Ntie-Kang F, Nwodo NJ, Adikwu MU. Structure-based virtual screening and molecular dynamics simulation studies to discover new SARS-CoV-2 main protease inhibitors. Sci Afr. 2021;14:e00970. https://doi.org/10.1016/j.sciaf.2021.e00970
72. Halgren TA, Murphy RB, Friesner RA, Beard HS, Frye LL, Pollard WT, et al. Glide: a new approach for rapid, accurate docking and scoring. 2. Enrichment factors in database screening. J Med Chem. 2004;47:1750–9. https://doi.org/10.1021/jm030644s
73. Daina A, Michielin O, Zoete V. SwissADME: a free web tool to evaluate pharmacokinetics, drug-likeness and medicinal chemistry friendliness of small molecules. Sci Rep. 2017;7:42717. https://doi.org/10.1038/srep42717
74. Pires DE, Blundell TL, Ascher DB. pkCSM: predicting small-molecule pharmacokinetic and toxicity properties using graph-based signatures. J Med Chem. 2015;58:4066–72. https://doi.org/10.1021/acs.jmedchem.5b00104